First observations of CH_4 and H_3^+ equatorial detached layers, as seen by JIRAM/Juno

A. Migliorini[1], B.M. Dinelli[2], C. Castagnoli[1], M.L. Moriconi[3], F. Altieri[1], S. Atreya[4], A. Adriani[1], A. Mura[1], F. Tosi[1], A. Moirano[1], G. Piccioni[1], D. Grassi[1], R. Sordini[1], R. Noschese[1], A. Cicchetti[1], S.J. Bolton[5], G. Sindoni[6], C. Plainaki[6], A. Olivieri[6], and the JIRAM Team

[1]IAPS-INAF, Istituto di Astrofisica e Planetologia Spaziali, Rome, Italy.

[2]CNR-ISAC, via Gobetti 101, Bologna, Italy.

[3]CNR-ISAC, via Fosso del Cavaliere, 100, Rome, Italy.

[4]Dept. of Climate and Space Sciences and Engineering, University of Michigan, Ann Arbor, Michigan, USA.

[5]Southwest Research Institute, San Antonio, Texas, USA.

[6]Italian Space Agency, Via del Politecnico, Rome, Italy.

Corresponding authors: Alessandra Migliorini (alessandra.migliorini@inaf.it), Bianca Maria Dinelli (bm.dinelli@isac.cnr.it)

Keypoints:

- Detection of CH_4 and H_3^+ emissions over the Jupiter's disc, as two well separated layers in the equatorial region.

- Both H_3^+ and methane spectral signatures can be reproduced by retrieving the temperature vertical profile or the vertical distributions of their Volume Mixing Ratios and temperatures simultaneously. When fitting only the VMR profiles only H_3^+ signature can be reproduced.
- The retrieved temperatures suggest that CH_4 is likely in non-LTE condition and the H_3^+ temperature profile shows a peak of 600-800 K at about 600 km.

Abstract:

In this work we present the detection of CH_4 and H_3^+ emissions in the atmosphere of Jupiter as two well separated layers, located, respectively, at a tangent altitudes of about 200 km and 500-600 km above the 1-bar level. We studied the vertical distribution of the two species retrieving their Volume Mixing Ratio (VMR) and temperature simultaneously or , allowing only one quantity to vary. From this analysis, it is not possible to firmly conclude if the observed H_3^+ and CH_4 features are due to an increase of their VMR or rather to variations of temperature of the two molecules. However, our retrieval indicates that CH_4 is in non-Local Thermal Equilibrium (non-LTE) condition, considering that the retrieved temperature values at about 300 km, where the maximum CH_4 concentration lies, is always about 100 K higher than the Galileo measurements.

We suggest that vertically propagating waves is the most likely explanation for the observed VMR and temperature variations in the JIRAM (Jovian InfraRed Auroral Mapper) data. Other possible phenomena could explain the observed evidences, for example a dynamical activity driving chemical species from lower layers towards the upper atmosphere, like the advection-diffusion processes responsible for the NH_3 enhancement observed by Juno/MWR (MicroWave Radiometer), or soft electrons precipitation, although a better modeling is required to confirm these hypothesis.

The characterization of CH_4 and H_3^+ species, simultaneously observed by JIRAM, offers the opportunity for better constraining the atmospheric models of Jupiter and understanding the planetary formation.

Plain Language Summary:

The Jovian Infrared Auroral Mapper (JIRAM) is the infrared (IR) imager and spectrometer on board the Juno mission, designed to investigate Jupiter's atmosphere. A key objective of JIRAM is the investigation of the minor species, like CH_4 and H_3^+ that are very important to understand the energy balance of the middle and upper atmosphere of Jupiter. These species have strong signatures in the 3.3-3.8 μm spectral region, well

within the nominal wavelength range of the instrument. We present the analysis of recent images and spectra obtained with JIRAM, in the period December 2018 to September 2020, plus additional measurements in March 2017, to study methane and H_3^+ vertical distribution at equatorial latitudes. The vertical distribution of the observed radiances shows that CH_4 is localized around 200 km above the 1-bar level, while a distinct layer due to H_3^+ is observed around 500-600 km (0.04-0.016 microbar). The observed vertical distribution and intensity variation of the two species are likely to be the result of vertically propagating waves. However, other possible phenomena can be invoked to explain these findings, like for example a dynamical process that drives chemical species from lower layers towards the upper atmosphere, or soft electrons precipitation, although a rigorous modeling is needed to confirm the latter hypothesis.

Keyword: Jupiter atmosphere, Spectroscopy, Juno mission

1. Introduction

The stratosphere of Jupiter is populated by minor species and ions. Among the molecules, H_3^+ and CH_4 show strong emission bands in the infrared used to evaluate the atmospheric and satellite interaction with energetic particles, which deposit energy in the upper atmosphere of Jupiter especially in the auroral region (Connerney et al., 1993; Clarke et al., 2002; Mura et al., 2017, 2018; Gérard et al., 2018). These species are also known to have a cooling effect on the atmosphere (Bougher et al., 2005; Koskinen et al., 2007; Stallard et al., 2017). Several H_3^+ emission lines, mainly due to the fundamental ν_2 band (Drossart et al., 1989; Giles et al., 2016), have been identified in the auroral region as well as at mid-equatorial latitudes (Miller et al., 1997; Ballester et al., 1994; Stallard et al., 2015; Migliorini et al., 2019). In particular, the wavelength region

around 3.4 μm can be exploited to study the auroral emissions due to H_3^+, because of its numerous and intense emission lines that can be identified above the deep methane absorption band. A thorough review of H_3^+ observations and properties for the giant planets can be found in Miller et al. (2020), while a new modeling interpretation strategy is reported in Moore et al. (2019).

The intensity of the H_3^+ emission at mid and equatorial latitudes is about 10 times fainter than in the auroral region (Ballester et al., 1994; Marten et al., 1994; Stallard et al., 2018) and its presence at latitudes outside the auroral region may be explained by the particle transport from the auroral region itself or by the precipitation of particles with energies of few keV (Lam et al., 1997). An optically thin layer of H_3^+ at the equator was clearly identified in the images acquired by the ProtoCAM infrared camera mounted on the Infrared Telescope Facility (IRTF), located at 700-750 km above the 600 mbar-level (Satoh and Connerney, 1999). More recently, a map of the H_3^+ emission in the region between ±60° in latitude was obtained using the data acquired at the NASA Infrared Telescope Facility, covering overall a period of 48 nights (Stallard et al., 2018). The same measurements revealed a dark ribbon within 15° of the jovigraphic equator, which is indicative of the magnetic equator of Jupiter.

Emissions at 3.3 μm due to methane have been identified for the first time using the NASA Infrared Telescope Facility (Kim et al., 1991) at the North polar region, while a bright small spot due to CH_4 has been detected near the South pole in the same spectral region by Kim et al. (2009). However, methane brightening in the polar regions was well studied in the 8-μm band (Kim et al., 1985; Drossart et al., 1993), reporting different behaviors in the North (Caldwell et al., 1983; Sada et al., 2003) and the South (Caldwell et al., 1988). The methane bright spots have different morphologies at 3- and 8-μm, and this could be explained by the different altitudes where the emissions occur (Lystrup et al., 2008). In addition, recent auroral observations reported that northern and southern emissions as imaged at 8-micron vary independently (Sinclair et al., 2017). High-resolution measurements in the 3.3-3.4 μm band pointed out that the observed methane molecules in the polar region are likely excited by energetic sources, possibly provided through auroral particle precipitation or Joule heating above the 1-μbar level (Kim et al., 2015), although further observations are required to discriminate between the two processes.

Faint emissions due to methane around 3.3 μm have been observed by the spectrometer embedded into the Jovian Infrared Auroral mapper (JIRAM) on board the Juno mission, in the polar regions, localized within the main auroral oval (Adriani et al., 2017; Moriconi et al., 2017) and with the Near Infrared Mapping Spectrometer (NIMS) on the Galileo spacecraft (Altieri et al., 2016). In the ultraviolet (UV), few signatures due to CH_4 were identified using the Ultraviolet Spectrograph (UVS) instrument on Juno (Bonfond et al., 2017). Other complex hydrocarbons, such as C_2H_4, C_3H_4 and C_6H_6 have been observed in the auroral regions of Jupiter (Sinclair et al., 2019).

Models predict the intensities and vertical distribution of both H_3^+ and methane (Grodent et al., 2001; Kim et al., 2014). Direct H_3^+ vertical profile measurements have been reported for the Southern auroral region, using NIRSPEC spectrometer observations on the Keck II telescope (Lystrup et al., 2008), showing a good agreement with models for ion densities; however, the measured exospheric temperature of 1450 K was about 150 K higher than predictions. More recent observations with the Infrared Camera and Spectrometer (IRCS) at the Subaru 8.2 m telescope allowed reconstructing the vertical profile of H_3^+ overtone and hot overtone, located at different altitude, at 700-900 km and 680-950 km above the 1-bar level, respectively (Uno et al., 2014).

While direct measurements have been reported for the H_3^+ vertical profile, at auroral and mid-equatorial latitudes (Miller et al., 1997; Ballester et al., 1994; Stallard et al., 2015; Migliorini et al., 2019; Dinelli et al., 2019), information for the CH_4 vertical distribution at equatorial latitudes is missing due to the emission faintness observed during the reported observations.

Recently, JIRAM, on board the Juno spacecraft, performed a dedicated limb observation campaign, starting from 24 May 2018 (perijove passage 13, PJ13). The high sensitivity of JIRAM and the capacity of measure both images and spectra in the 3-4 μm spectral range allowed the detection of the infrared emissions due to both CH_4 and H_3^+ close to the equator. In the present paper, we discuss the results obtained in the analysis of JIRAM limb observations, exploiting both images and spectra acquired during the Juno mission period December 2018-September 2020 (i.e. perijove passages 17 to 29), complemented with some spectra, acquired over Jupiter limb in March 2017 (perijove passage 5), in the equatorial region.

The paper is organized as follow: the data are presented in section 2, the description of the results in section 3. Discussion is provided in section 4, while conclusions are summarized in section 5.

2. Observations and data selection

2.1 Instrument description

The Jupiter InfraRed Auroral Mapper (JIRAM), onboard the Juno mission, combines an imager and a spectrometer in the same instrument (Adriani et al., 2017). The imager is composed of two broad-band filters, centered at 3.45 μm (L-band, bandpass 3.3-3.6 μm) and 4.85 μm (M-band, bandpass 4.5-5.0 μm), respectively, located in the same detector, which has a total dimension of 256 x 432 pixels in total, 256 being the number of lines and 432 the number of samples. The Instantaneous Field of View (IFOV) of each pixel is 0.01°, which implies a FOV of 5.87°x1.74° for each band of the imager.

The spectrometer covers the 2-5 μm spectral region, with a spectral sampling of about 9 nm; it is composed of a 256-pixels slit, and each pixel is expanded into 336 spectral channels, concurrently acquired. The spectral

slit is located within the M-band filter, and simultaneously commanded with the imager. However, due to the spinning movement of the spacecraft Juno, the JIRAM spectrometer is not able to acquire contiguous slit images of the target. This means that it is not possible to reconstruct the full scene observed by the imager at the same time. However, although with a sparse coverage, the observed spectra can be exploited to quantitatively study the distribution of CH_4 and H_3^+, along with other atmospheric properties. In case of limb measurements, the spectrometer enables to sample the atmosphere at different altitudes along the line of sight above the 1-bar level, using the pixels located outside the disk of the planet. More details of the observations are provided in the following.

The orbit attitude of the Juno spacecraft allowed the routinely observation of the equatorial region starting from orbit 13, while only sparse measurements are available during the previous orbits. In the present work, we include the analysis of images and spectra acquired during the perijove (PJ) passages 17 to 29 (December 2018 to September 2020), and a spectral sequence acquired during PJ 5 (March 2017).

Details of the analyzed images and spectra are provided in the sections 2.2 and 2.3, respectively.

2.2 JIRAM imager data and their analysis

In the limb campaign started with the orbit 13 (May 2018), a total of 89 images have been acquired by JIRAM. However, most of the data, especially during PJs 13, 14, 15, 16, and 19, were strongly contaminated by environmental radiations, and could not be used in the analysis. Hence, in this work we make use only of data with a good signal-to-noise ratio and poorly affected by radiations. The list of the images included in the present analysis is provided in Table 1. Planetocentric latitude and longitude of the center of each image in Sys III are reported.

Observation	Latitude	Longitude
181221-165438	15 N	226 E
181221-170111	3 N	210 E
181221-170613	6 S	200 E
181221-170838	1N	175 E
190212-172519	24N	162 E
190212-174018	4 S	119 E
190212-183613	15 S	109 E

190212-185616	23 S	117 E
190529-082044	20 N	325 E
190529-090148	3 S	309 E
190529-092207	10 S	308 E
190529-092711	12 S	307 E
190721-040901	6 S	65 E
190721-052832	16 S	50 E
190721-053834	19 S	53 E
190912-033605	8 N	53 E
190912-034305	4 N	46 E
190912-043957	3 S	344 E
190912-044557	5 S	350 E
190912-045627	11 S	3 E
190912-050629	16 S	7 E
191103-221838	11 N	186 E
191103-222537	4 S	167 E
191226-172503	24N	324 E
191226-173239	15 N	309 E
200217-174037	32 N	281 E
200217-174839	26 N	252 E
200217-175510	15 N	238 E
200410-140018	27 S	302 E
200410-140622	34 S	303 E
200602-100943	37 N	73 E
200602-101645	31 N	47 E
200602-102317	24 N	34 E
200602-111730	32 S	43 E
200602-112231	34 S	46 E

200725-060335	35 N	163 E
200725-062439	6 N	118 E
200725-071620	26 S	121 E
200725-072121	28 S	124 E
200725-073653	31 S	135 E
200916-020651	31 N	236 E
200916-021423	17 N	213 E
200916-033741	29 S	214 E

Table 1. List of JIRAM images (JIRAM-IMA) used in the present investigation. The first column identifies the image number (which is composed of the date – YYMMDD-HHMMSS), while information on planetocentric latitude (in deg) and longitude (in deg), is reported in columns 2 and 3, respectively.

Two examples of full JIRAM raw images are shown in Figure 1, where the L part is located at the top and the M one at the bottom of each image. It is possible to see the environmental radiation distributed across the whole image in the form of dark and bright pixels randomly distributed. This affects more the L band image, while lower radiation contamination is observed in the M image. In the case shown in Figure 1a, the radiation effect is not so dramatic to conceal the underlying emission pattern and therefore the image has been retained in the analysis, while the radiation recorded in the case of the image shown in Figure 1b is more dramatic, and hence JIRAM images like this one are not included in the analysis. In Figure 2 we reconstruct the tangent altitude of the L-band image shown in Figure 1a. The yellow line located at the right edge of the image (see Figure 2) indicates the location of the 1-bar level of Jupiter's atmosphere, while the red dashed line on the left indicates the tangent altitude at 1000 km above that level. Two layers are clearly visible in the image, the strongest one located closer to the 1-bar level and a fainter diffused layer above it. To infer the altitude of the two emission layers, a best-fit algorithm is applied. For each pixel of the data image (JIRAM-IMA), the line of sight is derived from SPICE kernels (Acton, 1996), and its contribution from different altitudes is evaluated. The reconstructed image (Figure 2b) is then simulated integrating the vertical profile along the line of sight. The resulting image is compared with the original data and the vertical profile is tuned until the best match is obtained (Figure 3). The reconstructed image differs from the original data by less than 5% and, considering that the pseudo-inverse matrix procedure is a linear operator, this percentage could be assumed as an upper limit for the uncertainty of the vertical profile, and hence we use it to calculate the error bars shown in Figure 3. This procedure can only be applied to the JIRAM imager channel measurements, as the best-fit algorithm requires a large number of pixels to converge to a physical solution. However, the comparison of this result with the geometric parameters of the spectral observations, shows that using the tangent altitudes of the spectrometer data to represent the intensity behavior as a function of vertical altitudes leads to an error of about

100 km. In fact, the topmost maximum is at about 500 km when using the tangent altitudes, and at 600 km in terms of vertical altitudes. These values must be considered when evaluating the correction to be applied to the tangent altitude values. The vertical profile (shown in Figure 3) of the intensity of the observed emissions obtained with the above described method shows two maxima, one at about 200 km, and one around 600 km. We attribute the first maximum to the methane emission and the second one to the H_3^+ emission.

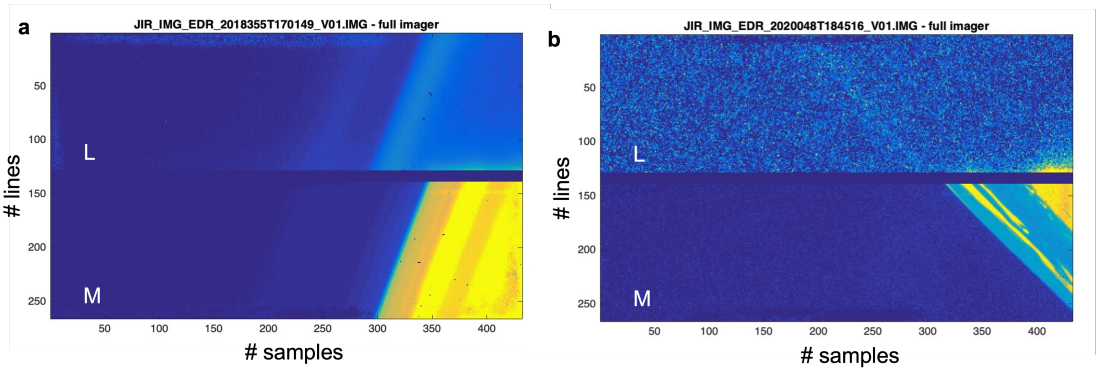

Figure 1. Example of JIRAM image (JIRAM-IMA) at limb. a: Full JIRAM-IMA, showing the L-band acquisition in the top and the M one at the bottom, affected by a low radiation. b: Another example of JIRAM-IMA at limb highly affected by radiation and not included in the analysis.

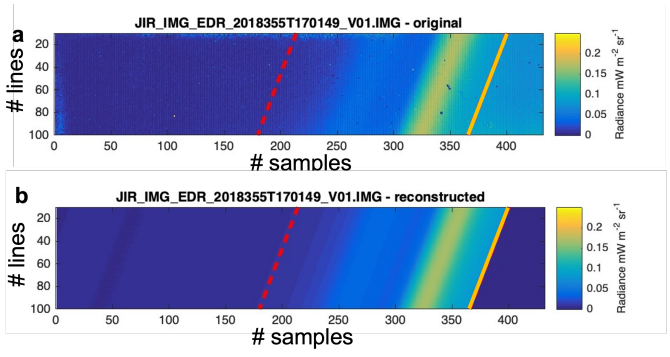

Figure 2. a: Same L-band JIRAM-IMA shown in Figure 1a, where the color coding indicates radiance. The yellow and red lines indicate the 1-bar level and 1000 km above it, respectively. b: Simulated image from the reconstructed vertical profile. The dark blue region at the bottom right, beyond the yellow line, signs the Jupiter 1-bar level surface.

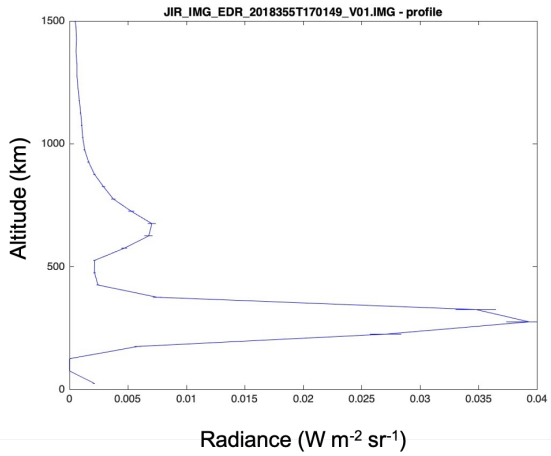

214

215 *Figure 3. Reconstructed vertical profile for JIRAM-IMA shown in Figure 1a obtained using the inversion*
216 *method. Uncertainty in the vertical profile is assumed to be the 5%, which corresponds to the maximum*
217 *difference between the original data and the reconstructed profile.*

218

219 Overall the data included in this analysis cover the planetocentric latitude region from 34°S to 37°N
220 (Figure 4). Most of the data are acquired at longitudes 120-240 E, with some sparse acquisitions at 40-60 E
221 and beyond 280 E.

222

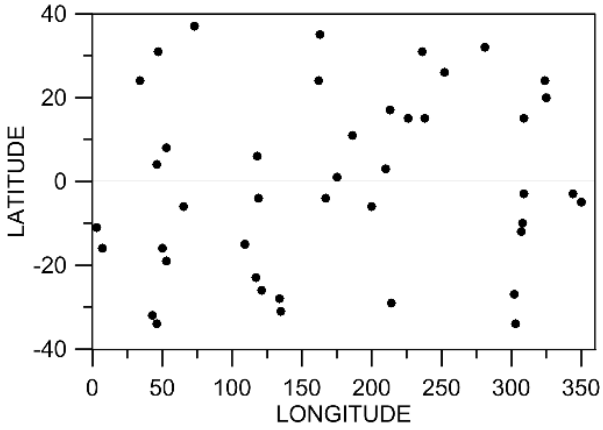

223

224 *Figure 4. Latitude-longitude dispersion of the JIRAM-IMA data included in the present work.*

225

226 2.3 JIRAM spectral data and spectral radiance analysis

227 To confirm the findings obtained with the analysis of the JIRAM-IMAs and the assignment of the intensity
228 peaks to either H_3^+ and CH_4, whose signatures are well resolved at JIRAM spectral resolution, spectra acquired

simultaneously to the images have also been examined. Spectral limb sequences have been selected following Migliorini et al. (2019) and Dinelli et al. (2019). The spectral acquisition of 21 Dec 2018 (17:01:11) is shown in Figure 5, with the latitude distribution as a reference. It was originally composed of seven slit images, three of which pointing the deep space and hence not shown here.

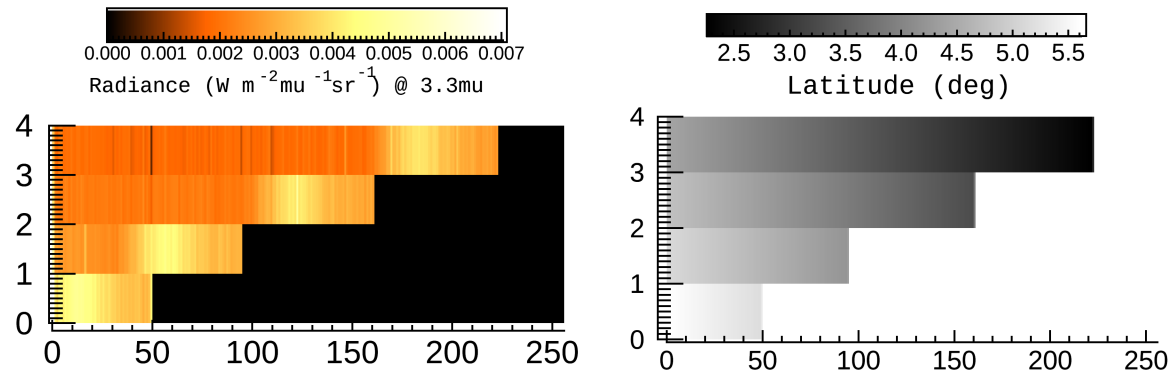

Fig 5. Spectral sequence of 21 Dec 2018 (17:01:11). Radiance at 3.32 µm, expressed in W $m^{-2}µm^{-1}$ sr^{-1}, is shown on the left for each slit image. The x-axis refers to the pixel along the slit, while the y-axis reports the temporal variation of the sequence (number of scans). The black region indicates the Jupiter's body masked at 1-bar level, as obtained from the reconstructed geometry. On the right side, planetocentric latitude values for the same image are shown.

Although limb measurements aligned along a vertical to Jupiter 1 bar surface are not possible with the JIRAM spectrometer, due to pointing constraints, we verified that each pixel along the slit acquisition was scanning the atmosphere within 1 deg of latitude and longitude. For the dataset used in this work, 1 deg in terms of latitude and longitude corresponds to a box of about 1246 x 1244 km at a latitude of 4°.

Since JIRAM spectra are affected by a sawtooth shape (odd-even pattern) due to the measurement strategy, the faint emissions due to both H_3^+ and CH_4 was in some cases hidden by the background noise. For this reason, each spectrum has been corrected to attenuate, and in some cases remove, the odd-even pattern. This correction is based on the fact that the intensities of the odd and even channels of the spectrometer are consistently shifted, and show a sawtooth pattern, that is more pronounced in case of a low signal. To correct this effect, two spline curves are fitted to the odd and even channels separately, and then interpolated onto the original grid of spectral bands, obtaining two separate spectra. These spectra are finally averaged to obtain the cleaned spectrum. This correction has allowed to recover spectra that were not used in the first analysis of JIRAM limb spectra (see Migliorini et al., 2019).

# JIRAM section	Latitude (deg)	Longitude (deg)	Solar Zenith Angle
Limb 1	6 N	177 E	90
Limb 2	4 N	176 E	90
Limb 3	1.5 N	175 E	90

Table 2. Geometric parameters of the analyzed spectra.

To test our hypothesis on the altitude of the CH_4 and H_3^+ emissions identified in the imager data, we investigated the selected spectral limb sequences, in order to reconstruct in terms of radiance the vertical distribution of the two species separately.

Figure 6 shows the vertical distribution of the intensity of the CH_4 and H_3^+ emissions for the spectral image on 21 Dec 2018 (3.8 N and 176 E), shown in Figure 5. The profiles are obtained considering the integrated intensity in the bands 3.29-3.34 μm (for CH_4) and 3.51-3.69 μm (for H_3^+), over altitude bins 100 km wide. The integrated radiances from the spectra with tangent altitude within the limits of each bin have been averaged and plotted with their statistical error. The wavelength range for H_3^+ has been chosen to include the strongest H_3^+ bands observed in the spectra and avoid any contamination from other species or background noise. The averaged intensities have been corrected for the background (continuum) signal. It can be clearly seen in the figure that the JIRAM-IMA intensity peak at 200 km belongs to methane, while the other peak at about 500-600 km can be attributed to H_3^+.

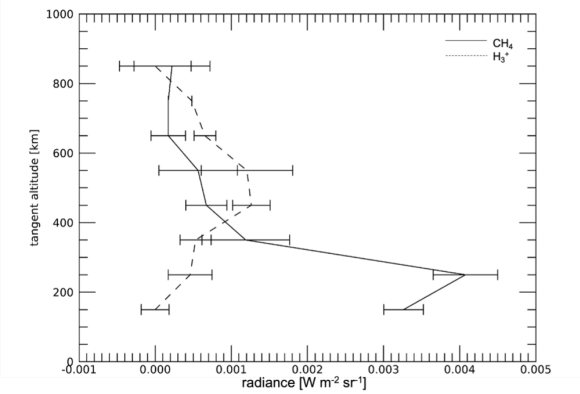

Figure 6. Vertical profile of integrated radiances for JIRAM spectral bands 3.29-3.34 μm and 3.51-3.69 μm, for CH_4 and H_3^+, respectively, in altitude bins 100 km wide. Data refer to JIRAM observation acquired on 21 Dec 2018.

2.4 Quantitative analysis of the spectra

The selected limb sequences have been analyzed to retrieve the vertical distributions of methane, H_3^+ and their temperatures. Details of the retrieval process are provided in the following subsections. We have initially considered three limb scans, acquired during the sequence of observations on 21 Dec 2018, 17:01:11 (shown in Figure 5), with the geometry parameters reported in Table 2. To confirm the results obtained by this first analysis, we have then included in the retrieval a set of 23 limb observations acquired on 27 March 2017 (PJ5), originally used for the derivation of the H_3^+ distribution at equatorial and mid latitudes in Migliorini et al. (2019). The 23 sequences covered the latitude region from 5°S to 37°N, and the longitude interval from 258 E to 290 E. Despite the number of spectra and the vertical coverage and resolution of these limb sequences are very different from the ones acquired on 21 December 2018, a clear methane emission was visible at tangent altitudes below 300 km. This was the reason that made the previous analysis, dedicated to H_3^+ only, discard all the observations below that altitude. All the other limb observations analyzed in Migliorini et al. (2019) were covering higher latitudes and no methane emission was visible.

2.4.1 Retrieval code and limb measurement

The measurements acquired with the spectrometer have been used to quantitatively retrieve the vertical distribution of CH_4 and H_3^+ Volume Mixing Ratio (VMR) along with the temperature (T). Each pixel of the spectrometer's slit, located outside the Jupiter's disk, samples the atmosphere at more than one altitude above the 1 bar level, along the instrument line of sight (LOS) crossing the atmospheric shells. The minimum altitude reached by the LOS of each pixel is called the 'tangent altitude'. We call limb sequence the set of spectra, acquired by the spectrometer in a single measurement session, relative to the pixels outside the Jupiter disk. While the limb sequences acquired on 27 March 2017 are made of few spectra with tangent altitude steps of the order of 100 km, in the three limb sequences acquired on 21 December 2018, the slit had more than 100 pixels sampling Jupiter's limb, with tangent altitude steps on the order of tens of km. The Forward Model (FM), inside the retrieval code, basically the same used in Dinelli et al. (2019) and Migliorini et al. (2019), numerically solves the integral of the radiative transfer along the instrument LOS in a curved atmosphere. The spectrum is computed with a line-by-line procedure. The simulation of more than 100 spectra has been proven to be too expensive in terms of computing time and memory allocation, therefore, we decided to divide the vertical extension of each slit measured in 2018 into bins of 50 km and to average all those spectra (typically 8) whose tangent altitudes fell into the bin. This trick reduced the number of spectra to be analyzed for each slit and improved the S/N ratio of the observations. To avoid contamination of anomalous signals (i.e. spikes due to radiation) in the final average, we used the median instead of the mean value of the observed radiances at each wavelength. In the forward model inside the retrieval code, Jupiter's atmosphere is assumed vertically

inhomogeneous and composed of curved layers (equidistant from Jupiter 1 bar surface) homogeneous in the horizontal direction only. This implies that its composition, pressure and temperature are allowed to vary with altitude within each layer. The simulation of the spectra is performed on a very fine frequency grid (0.0005 cm^{-1}), to take correctly into account all the emission and absorption processes of the single spectral lines. The high-resolution spectra are then convolved with JIRAM instrumental response function (a gaussian) and the Field of View response function. The odd-even correction, implemented in the same way as for the measurement treatment reported above, is finally applied to the simulated spectra. The derivatives of the spectra with respect to the volume mixing ratio (VMR Jacobians) are analytically computed at the same time of the spectrum and the same convolutions and odd-even corrections are applied, while the temperature Jacobians are numerically computed. In the simulations, we assume Jupiter atmosphere made of H_3^+ and methane only, since all other molecules have small or negligible signal in the considered spectral region. The pressure values at the altitude above the 1-bar level are taken from Seiff et al. (1998).

Despite the FM can represent deviations from the Local Thermal Equilibrium (LTE), in our analyses, H_3^+ and CH_4 are assumed in LTE at the considered altitudes. Therefore, the retrieved temperatures reported in this analysis must be considered as effective values, especially for methane. The treatment of the non-LTE requires an accurate modelling of collisional and radiative processes that lead to the population of the energy levels involved in the transitions responsible for the observed emissions. This model is currently not available to our team and will be the subject of a future work.

Applying the retrieval code, we had to consider that in the analyzed spectral region some of the lines of H_3^+ are almost superimposed to the Q-branch of methane, and that the spectral measurements clearly showed that the emission recorded in the region above 400 km was only due to H_3^+, while the spectra at lower altitudes were dominated by the methane emission. If the whole vertical coverage of the limb sequences is merged in a single analysis, strong correlations between the H_3^+ and CH_4 vertical distributions arise. To avoid them, we performed the retrievals into two steps: in the first step we retrieved the vertical distributions of temperature and H_3^+ VMR in the vertical region from 450 to 800 km using the spectra with tangent altitudes above 400 km; in the second step, the results of the previous calculations were fixed in the subsequent retrieval, where, along with the vertical distribution of temperature, only the CH_4 distribution was retrieved over a vertical range from 100 to 400 km, using the limb observations with tangent altitudes below 450 km. The final temperature profile was then obtained merging the results of the two steps of the analysis for each limb sequence. To easy the comparison of the results, the same procedure was applied to subsequent analyses where only the temperature profile (that will represent the H_3^+ temperature above 400 km and the methane temperature below 400 km) or the VMR alone was retrieved.

The retrieval was performed using the same technique reported in Migliorini et al. (2019) and Dinelli et al. (2019). We used the global fit technique (Carlotti et al., 1988), and a Bayesian approach (Optimal estimation, Rodgers 2000) with an iterative Gauss-Newton procedure.

The retrieval process is applied to the spectral region from 3.2 to 3.8 μm, because in this range the spectrum is dominated by the H_3^+ and CH_4 emissions, while solar scattering can be almost neglected. On the other hand, the treatment of the scattering by particles and molecules, which are important outside this range, is not included in the FM internal to the retrieval code. The vertical variation of the temperature and the vertical distribution of the VMR of the considered molecule are free parameters, and are the output of the retrieval code. In addition, a constant wavelength shift, also variable in the retrieval process, is applied to account for possible second order calibration errors of the wavelength. Any other instrumental effect, which can contribute as an offset to the spectrum, was evaluated in the portions of the spectra which are free from molecular emissions and just a scaling factor (variable with altitude only in the methane vertical range) was retrieved.

The same a-priori profiles were used for all the analyses, in order to ensure that the observed variability was real and not related to a variable a-priori information. The a-priori profile for temperature was the one reported by Seiff et al. (1998) and was also used as initial guess in the vertical range from 400 to 800 km. Below 400 km, the temperature profile of Seiff did not allow to simulate the methane emission, since the LTE signal of methane at temperatures below 200 K in the 3 μm frequency range is close to zero. Therefore, we added a constant value of 50 K to the Seiff's profile in the altitude range from 100 to 350 km and used it as initial guess. The a-priori profiles used for methane is the model 3 reported by Moses et al. (2005), while for H_3^+ we used a custom-made profile. Both CH_4 and H_3^+ a-priori profiles, along with the temperature, are reported in Table 3. The a-priori errors for temperature and VMRs were assumed to be equal to 100 K and 100%, respectively, with a constant additive bias equal to 0.01 ppmv for H_3^+ and 1 ppmv for CH_4, introduced to avoid strong constraints due to VMR estimates being too small. The vertical retrieval grid for T and VMRs was uniformly distributed, with steps of 50 km. As already said, H_3^+ and CH_4 are retrieved separately in the altitudes ranges 450-800 km and 100-400 km respectively. H_3^+ spectroscopic data are the ones available at the web site http://h3plus.uiuc.edu/database/ (Lindsay and McCall, 2001), while for methane the spectroscopic data were taken from HITRAN2016 (Gordon et al., 2017), available online upon registration).

Altitude	CH_4 VMR (ppmv)	H_3^+ VMR (ppmv)	Temperature (K)
800	2.64e-11	0.4184E-01	877.2
750	2.336e-10	0.3493E-01	826.0
700	2.841e-9	0.2566E-01	741.0
650	4.207e-8	0.1927E-01	686.5
600	5.62e-7	0.1353E-01	669.8
550	8.357e-6	0.7785E-02	653.2
500	2.183e-4	0.2042E-02	545.9
450	5.827e-3	0.1541E-02	509.4

400	0.2341	0.1040E-02	370.2
350	11.95	0.9012E-03	265.1
300	165.7	0.8501E-03	227.6
250	616.8	0.8447E-03	203.3
200	1062.0	0.8447E-03	208.2
150	1454.0	0.8447E-03	214.6
100	1707.0	0.8477E-03	208.1

Table 3. A-priori profiles for the retrieved quantities.

3. Results

3.1 Imager

The band width of the L-band of JIRAM imager covers both CH_4 and H_3^+ emission lines, therefore their signals contribute to produce the observed images. The reported images clearly show that two well separated layers are present (see for example Figure 1a), one very bright at low altitudes and one fainter at high altitudes.

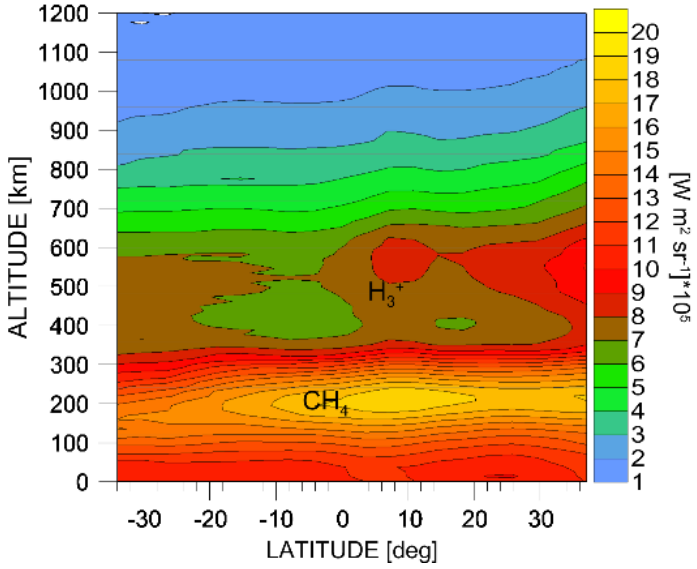

Figure 7. Map of CH_4 and H_3^+ emissions obtained with the L-band images acquired with JIRAM from 21 Dec 2018 to 3 Nov 2019.

Figure 7 shows the radiance map as a function of altitude, in the latitude range 34°S-37°N, obtained by considering only the L-band JIRAM images not contaminated by radiation, listed in Table 1. In this map, all longitudes are merged together, while the resolution in latitude is better than 5 deg. The resolution in altitude varies from a minimum of 4 km to a maximum of 75 km (due to the different resolution among different JIRAM intensity profiles) with an average resolution of 9 km. Errors in the determination of latitude and longitude are ±1deg.

According to section 2.3, the relative maximum of intensity, located at about 200 km, is clearly due to the CH_4 emission, while the one peaking at about 500 km, can be attributed to H_3^+. CH_4 shows a clear maximum in radiance between 6°N and 10°N, with values decreasing with increasing latitude almost symmetrically with respect to the equator. H_3^+ has a slightly fainter maximum, located at the same latitude.

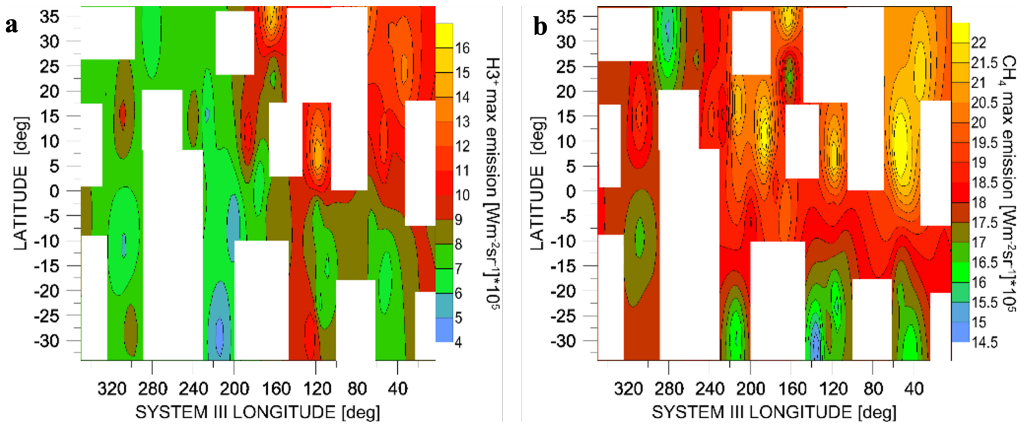

Figure 8. a: Map of H_3^+ emission obtained by considering only the data with a tangent altitude greater than 350 km, acquired with JIRAM-IMA from 21 Dec 2018 to 3 Nov 2019, in terms of longitude and latitude. B: Latitude-longitude distribution of CH_4 emission obtained using the same data, selected for tangent altitudes lower than 350 km.

If we consider the longitude (Figure 8), higher concentrations of CH_4 are present at different locations around the planet, and particularly at 50 E, 120 E and 190 E (Sys III). The CH_4 map (Figure 8b) in this case is obtained considering only radiance for tangent altitudes below 400 km in the L-band images listed in Table1. At 120 E and 190 E, relative maxima of H_3^+, obtained using only the L-band image portions with tangent altitudes above 400 km and shown in Figure 8a, are observed as well, but not at 50 E. However, since the longitudinal coverage of our measurements is very sparse, any consideration with this parameter is difficult to be explored. In the case we consider only data acquired up to May 2019 (PJ20), the scenario is a little bit different, and the two species show a strong local maximum of emission close to 4°N, with an additional local maximum beyond 15°N above 500 km due to H_3^+. Although this factor alone is not sufficient to explain the

observed shift of the maximum towards higher latitudes, a more uniform coverage in longitude would clarify the trend.

3.2 Retrievals

The results of the analysis of the selected limb spectra with the retrieval code described in session 2.4.1 are reported in Figs. 9 to 12. The single limb sequences have been analyzed separately performing three different retrievals: first both VMR and temperature were allowed to vary (configuration 1), then only temperature (keeping the VMR fixed at their a-priori values – configuration 2) or VMR (keeping the temperature at Seiff et al. (1998)'s values – configuration 3) have been retrieved. The average temperatures obtained in configuration 1 for the observations in the two separate orbits are plotted in the left panel of Figure 9, along with the a-priori profile used. We can see in the figure (left panel) that the temperatures obtained from the observations acquired during the two orbits are very similar, therefore we feel that we can discuss the results of the different retrieval configurations merging all the retrieved values in a single plot. The right panel of Figure 9 shows the comparison of the average temperature profiles obtained with the retrieval configurations 1 and 2.

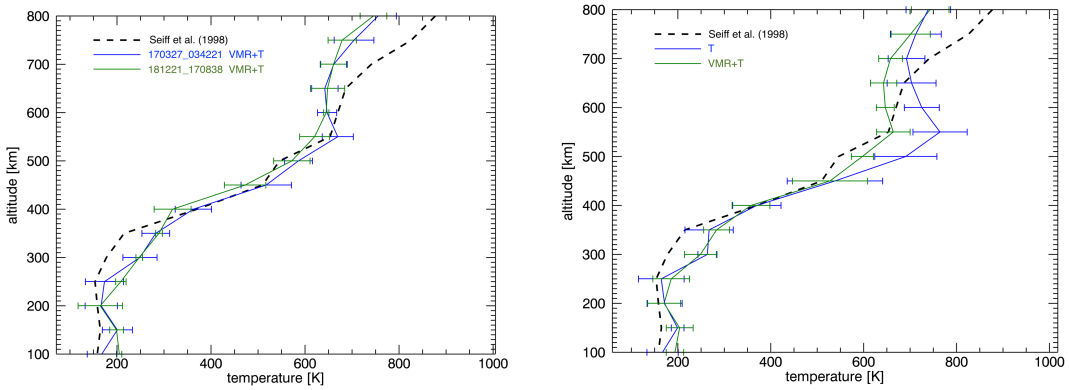

Figure 9. Comparison of the average temperature retrieved in the two considered orbits (left panel) and in retrieval configurations 1 and 2 (right panel). The dashed line represents the a-priori profile taken from Seiff et al. (1998). The error bars represent the standard deviation of the average.

While the temperature profile retrieved in the two configurations is very similar in the altitude range where the methane peak is present (below 400 km), in the altitude range where H_3^+ peaks the results are different, with a smaller standard deviation in the case of configuration 1. However, in both configurations we find a peak of the temperature at about 550 km, lower temperatures than the ones reported in Seiff et al. (1998) above

650 km and higher values with respect to the Galileo's profile (Seiff et al., 1998) in the altitude range from 350 to 250 km.

In Figure 10, we compare the maps of the retrieved temperatures for configurations 1 (left panel) and 2 (right panel). The maps have been obtained by merging the observations of the two orbits and averaging the retrieved profiles in latitude bins of 3 deg. When H_3^+ VMR is not retrieved, the peak of the emission at 550-600 km is reproduced by an enhancement in the local temperature, while the same does not apply to the vertical range where CH_4 is retrieved. In fact, the temperature distribution below 450 km is similar in both retrieval configurations. However, when retrieving the CH_4 VMR (both in configurations 1 and 3), we see an anomalous decrease in its VMR below 200 km, as shown in Figure 11, decrease that is not compliant to the various models of Jupiter's atmospheric composition, which suggest a larger methane VMR at lower altitudes. This behavior could be an indication of the non-LTE nature of the observed methane emission; indeed, when the temperatures are fixed to the Seiff's values and only the VMR is retrieved (configuration 3), the retrieval fails to reproduce the methane emission lines in most of the vertical retrieval range. The retrieval behavior in the vertical range of H_3^+ is different: in all the three configurations we can reproduce the H_3^+ signal within the retrieval error. Therefore, just using JIRAM limb observations, we cannot conclude if the enhanced signal of H_3^+ in the equatorial region is due to an enhancement of its concentration, of its temperature or both. The results of the retrieval of H_3^+ VMR in configurations 1 and 3 are shown in Figure 12.

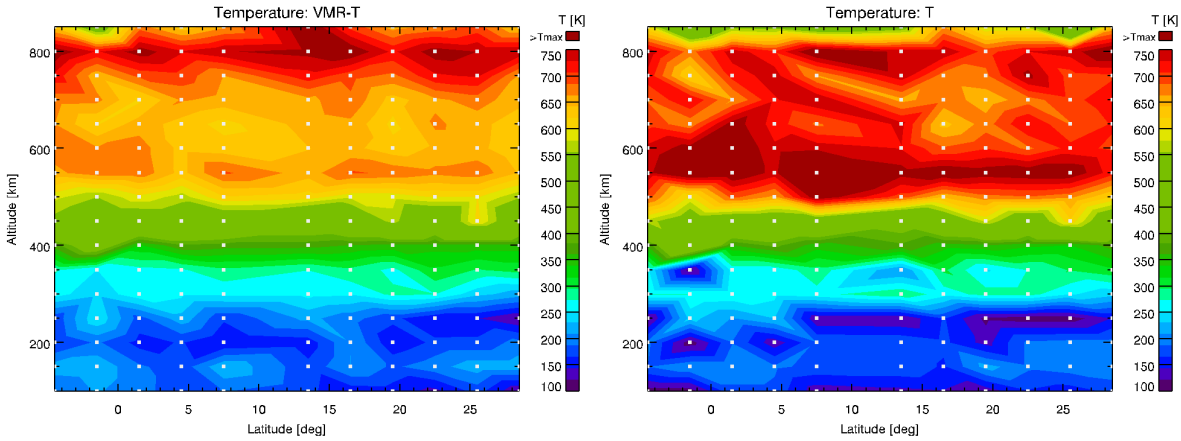

Figure 10. Map of the vertical distribution of temperature as a function of latitude in configuration 1 (left panel) and 2 (right panel).

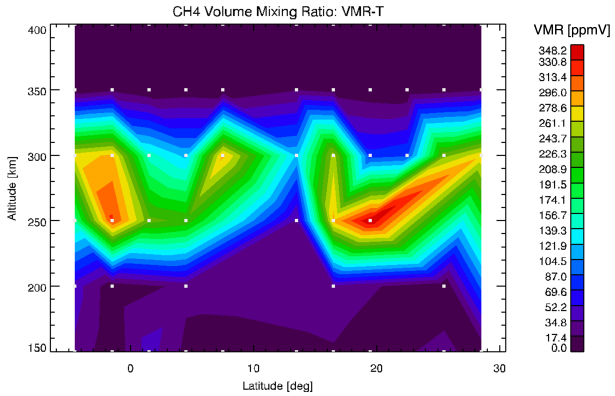

449

450 *Figure 11. Map of methane VMR as a function of altitude and latitude obtained with the retrieval*

451 *configuration 1.*

452

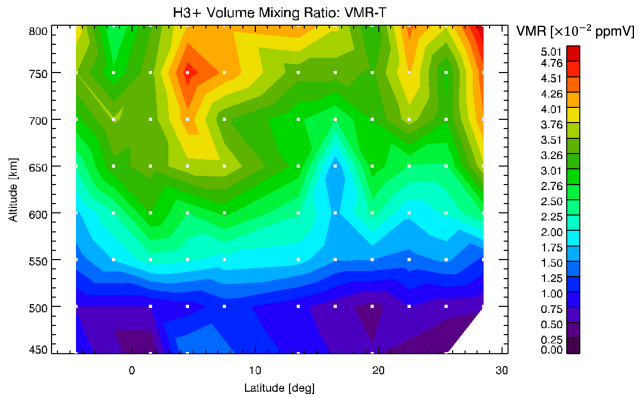

453

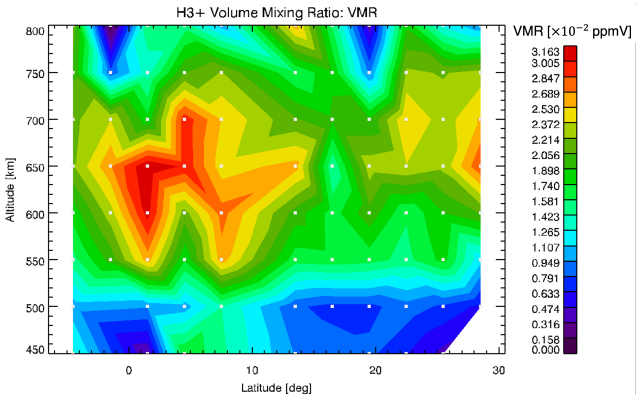

454

455 *Figure 12. Map of H_3^+ VMR as a function of altitude and latitude, for retrieval configuration 1 (left) and*

456 *configuration 3 (right).*

457

458 **4 Discussion**

The high spatial resolution of JIRAM during the limb observing campaign allowed the simultaneous identification for the first time of two layers, located at about 200 and 500 km respectively, and compatible with CH_4 and H_3^+ emissions. The spectral capability of JIRAM was used to investigate the zonal and vertical distribution of the two species. This showed that the maximum enhancements of both CH_4 and H_3^+ are located at about the same latitude, at 6-10°N with respect to the equator, as retrieved from the global map in Figure 7.

The only way to separate the H_3^+ emissions from the CH_4 ones in JIRAM L-band images is to use the information provided by the spectrometer that indicates that the two species are vertically separated, as shown in Figure 6. Therefore, we can use the imager data above 350 km to study the H_3^+ contribution, while the data below that altitude can be used to study the methane distribution. The maps in Figure 8 show the distribution of the radiances (integrated over the considered altitude range) as a function of latitude and longitude (Figure 8a for H_3^+ and Figure 8b for CH_4). We see that the two molecules have a different distribution of max and min radiance values. In addition, the H_3^+ radiance distribution is compatible with the global map obtained from ground observations and the magnetic equator reported in Stallard et al. (2018), despite the very patchy longitudinal coverage of JIRAM spectral data, as shown in Figure 13.

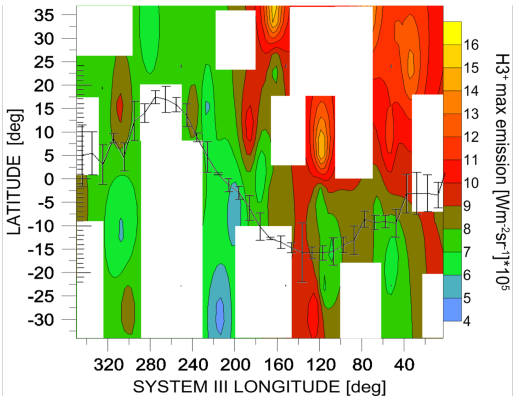

Figure 13. Same as Figure 8a, with the magnetic equator line superposed (from Stallard et al., 2018).

JIRAM limb measurements allowed the simultaneous observations of the emissions from CH_4 and H_3^+ and the investigation of their vertical distribution. We know that the CH_4 emission in the auroral region is expected to occur at 200-300 km, depending on the initial assumptions (Kim et al., 2014). The maximum of the H_3^+ emission has been reported at about 700-900 km and 680-950 km for the H_3^+ overtone and hot overtone in the Northern auroral region (Lystrup et al., 2008; Uno et al., 2014), while an altitude between 300 and 500 km above the 1-bar level has been inferred at mid latitudes from Cassini/VIMS data (Stallard et al., 2015). The radiative transfer code applied to our selected spectral measurements at equatorial latitudes in limb geometry permitted the exploration of VMR and temperature characteristics of the two species. When the methane VMR is retrieved together with its temperature, it results with a peak value ranging from 240 to 340 ppmV in the

vertical region of 250-350 km, at all the considered latitudes (Figure 11). However, its value becomes very low at altitudes below 250 km, in contrast with what predicted by Moses et al. (2005). The retrieved VMR of H_3^+ has a peak value of about 4.5 x 10^{-2} ppmV, at about 4°N, located at 750 km when temperature and VMR are simultaneously retrieved (configuration 1), while it assumes a lower value (3 x 10^{-2} ppmV) and is located at lower altitude (600 km) if the temperature profile is fixed to the Seiff's values (configuration 2, see Figure 12). In a previous analysis of JIRAM limb measurements, Migliorini et al. (2019) reported a H_3^+ VMR of about 1.4 x 10^{-3} ppmV at 5°N, located close to 600 km, compatible with the measurements presented in this work. In addition, values of about 8 x 10^{-4} ppmV at 500 km above the 1-bar level were obtained at 40°S (Migliorini et al., 2019), values that are about 20 times lower than the measurement reported in the equatorial region. JIRAM data indicate that there is an enhancement either in the H_3^+ concentration or in its temperature on in both of them towards the equator. Our retrieved values of temperature and VMR are overall in agreement with the revised models for the outer planets (Moore et al., 2019). In addition, an asymmetric distribution of H_3^+ VMR is reported in Migliorini et al. (2019), being more intense in the southern hemisphere above 500 km.

The variability in H_3^+ and CH_4 signals could be just a consequence of their temperature variations, as reported in section 2.4.1 and shown in Figure 10. The retrieved H_3^+ temperature has a local maximum at about 600 km either when it is retrieved alone or when also the H_3^+ VMR is retrieved. Its peak value is in the range of 600-800 K, and it is lower than Galileo's measurements above 700 km in both retrieval configurations. The temperature retrieved from CH_4 emission in 1 and 2 configurations is always larger than Galileo's measurements in the vertical region from 250 to 350 km.

It has been shown that stratospheric oscillations and quasi-quadrennial oscillation occur in the Jovian atmosphere (Cosentino et al., 2017). Temperature anomalies, observed with the Texas Echelon Cross Echelle Spectrograph (TEXES), are well reproduced by the model assuming stochastic waves produced from convection. The observed anomaly progresses also with time, showing a local maximum at equator in 2013 data, which turns to a minimum in the data obtained in late 2014 and beginning of 2015.

In O'Donoghue et al. (2016) it is shown how wavy activity is responsible of the H_3^+ enhancement above the Great Red Spot (GRS). This emission enhancement was explained with acoustic waves resulting from the turbulent troposphere around the GRS, which deposited their energy in the form of heat after breaking. The same phenomenon could also be explained with Joule heating, resulting from the GRS vorticity (Ray et al., 2019). Similar effects could be playing in the Jupiter's atmosphere and be the cause of the observed features in the JIRAM data reported in our analysis.

In Cosentino et al. (2017), it is proposed that convection is an important driver for oscillations in gas giant atmospheres. By chance, the pattern observed in the JIRAM imager data recalls the NH_3 concentration map, as retrieved with MWR onboard Juno (Li et al., 2017), although the latter data sound a much deeper pressure region (1-60 bars). Ammonia, as well as water, are found to be depleted at all latitudes in the range 40° north and south, with an exception at equatorial latitudes, where the two species are uniformly mixed (Li et al., 2017,

2020). The observed high concentration of NH_3 is consistent with the low temperature values recorded with the antenna. A similar NH_3 distribution is reported during all perijove passages with MWR, confirming the persistent behavior of the species (Li et al., 2020). However, methane and H_3^+ emissions show, with respect to NH_3 high concentration, a maximum slightly shifted towards the northern latitudes in case recent data are considered, while there is a latitude matching with the location of NH_3 high concentration in case of data acquired through May 2019 are included in the analysis. We don't have an explanation for this shift, and further analysis of future JIRAM data with a more uniform longitude coverage would be helpful.

The CH4 enhancement in the JIRAM data is in agreement with some wave activity and heat deposition at discrete altitudes or linked to an upwelling mechanism, quite stable with time, although modeling would be required for a confirmation. CH_4 and H_3^+ maps, being an average of measurements obtained in a time span of 18 months, show a mean picture, while NH_3 distribution does not show variations from orbit to orbit. Further measurements, extending to mid and high latitudes on both hemispheres, will help confirming this behavior.

The temperature retrieved from the methane emission is about 100 K larger than Galileo's measurements in the vertical range from 250 to 350 km. Moreover, the behavior of the retrieval of CH_4 VMR in configurations 1 and 3 suggests that its emission is likely in non-LTE condition and that the measured temperature should be regarded as a vibrational temperature of methane. We can speculate that the vibrational levels involved in the emission itself are populated by collisions with energetic particles or solar pumping, although further measurements, especially looking to the night side of Jupiter, are required to confirm this hypothesis. Despite our forward model can reproduce the signal generated by molecules in non-LTE, a proper treatment of this phenomenon requires to model all the collisional and radiative processes involving the methane molecules. Since we do not have this model, this aspect will be studied in a future work.

Excitation by soft electrons may be another possibility to explain the JIRAM observations, considering that the temperatures in the region of the methane layer at 300 km (and throughout the stratosphere) are about 100 K larger than the temperatures measured by the Galileo probe (Seiff et al., 1998) in approximately the same equatorial region (Figure 9), but this hypothesis requires a dedicated model to be confirmed, which is outside the scope of the present paper. Such an increase is unrelated to any solar cycle variations in the solar UV or photoelectron flux. Moreover, the CH_4 density in the layer at 300 km does not resemble at all the CH_4 density in the well-mixed region of the stratosphere (Atreya et al., 1999). Unlike the condensibles, NH_3 and H_2O, methane is expected to be uniformly mixed to ~300 km, above which photochemistry begins to deplete it somewhat below the methane homopause. Thus, the JIRAM observations of a CH_4 layer in the middle stratosphere and corresponding higher temperatures require a different disequilibration process than photochemistry. The concept of soft electrons was introduced to explain Jupiter's high exospheric temperature measured on Pioneer 10 and 11 (Hunten and Dessler, 1977), and may be an alternative to gravity waves or an additional source of heating. Soft electrons have also been proposed for explaining the hydrogen electro-glow in the non-auroral region at the giant planets (e.g. Atreya, 1987). The distribution of soft electron energy deposition in the atmosphere and the excitation of CH_4 would depend on the origin, power spectrum and the

557 angular dependence of soft electrons, which are presently not characterized. Detailed modeling of this idea is
558 beyond the scope of this paper and will be further tested in a future dedicated work.

559 New observations at limb, planned during the Juno nominal and extended mission, will help extend the
560 observed maps and shed further light on the possible Jovian atmospheric circulation.

561

562 **5 Conclusions**

563 Recent JIRAM measurements allowed the investigation of limb-view emissions of minor species at
564 Jupiter's equatorial region. Dedicated observing campaigns in limb viewing geometry, during orbits 17 to 29
565 (covering the period December 2018 to September 2020), explored the latitude range 34°S-37°N, and showed
566 for the first time two separate layers due to CH_4 and H_3^+, as seen at limb.

567 Limb measurements with the resolution of few km per pixel, as those acquired with JIRAM during these
568 dedicated campaigns, are quite innovative and show a wealth of details never obtained for Jupiter by previous
569 space missions. These observed features are quite unexpected and can provide the scientific community with
570 important hints for future observations and models.

571 We took advantage of the limb measurements with the L-band JIRAM imager to investigate the zonal and
572 vertical distribution of the CH_4 and H_3^+ signals at equatorial latitudes.

573 The identification of the two layers, made possible by the unique view of JIRAM, is quite new and
574 represents an important piece of information to refine circulation models. These emissions, although well
575 studied from ground and space, are only partly characterized. Recent JIRAM observations allowed deriving
576 the altitude of H_3^+ emission, as observed at limb with the JIRAM spectral channel (Migliorini et al., 2019;
577 Dinelli et al., 2019). However, CH_4, although inferred through its fundamental band emission at 3.3 μm,
578 superposed to the H_3^+ band at the same wavelength, was not directly observed at equatorial latitudes. Methane
579 had to be added in the retrievals to properly fit the auroral emissions spectra, observed in Nadir view by JIRAM
580 (Dinelli et al., 2017; Adriani et al., 2017; Moriconi et al., 2017). The measurements, used in the present work,
581 clearly show for the first time a CH_4 emission layer, located at about 200 km above the 1-bar level, and below
582 the H_3^+ layer where emissions are observed at about 500 km.

583 Both H_3^+ and CH_4 spectral signatures can be reproduced by retrieving the temperature vertical profile or
584 the vertical distributions of their VMRs and temperatures simultaneously. When fitting only the VMR profiles
585 only the H_3^+ signature can be reproduced.

586 The results of the retrievals exercises show that the T profile below 400 km does not change if data of
587 different orbits are separately examined or different retrieval configurations are used, and consistently show
588 an increase on the order of 100 K with respect to the Seiff's profile at about 300 km. In the vertical region

above 400 km, the resulting T profile shows a peak at about 550 km that is higher in the case the VMRs are kept fixed in the retrieval process. Regarding the H_3^+ profile, the VMR distribution is similar in the considered cases, but the peak shifts towards higher altitudes and has a higher value in the configuration where VMR and T can vary in the retrieval process.

From these results, it is not possible to firmly conclude if the observed H_3^+ features are due to a real increase of their VMR or rather to variation of temperature of the two molecules because the retrieval procedure is able to reproduce JIRAM data in all retrieval configurations.

Our analysis definitely suggests that CH_4 is in non-LTE condition, based on the retrieved temperature values and on the impossibility to reproduce the obtained signal at the Galileo's temperatures. An investigation on the non-LTE conditions of methane will be the subject of a future work with a dedicated model. Vertically propagating waves are the most plausible explanation to describe the VMR and/or temperature variations of CH_4 and H_3^+ at mid and equatorial latitudes in the JIRAM data, in analogy with previous observations (Cosentino et al., 2017; O'Donoghue et al., 2019). We also find that H_3^+ and CH_4 emission distribution mimics somehow the behavior of NH_3, observed with MWR onboard Juno (Li et al., 2020). However, considering that NH_3 is located well below the 1-bar level at a different pressure level than the species analyzed in the present work, it is quite difficult to see a direct correlation between the two distributions. We can also speculate that soft electron precipitation might cause the observed CH_4 distribution, in analogy with previous explanations to the Pioneer measurements of the high exosphere of Jupiter (Hunten and Dessler, 1977), and the electroglow at the giant planets (e.g. Atreya, 1987). However, more accurate modelling of magnetospheric and electronic precipitation is required to confirm this hypothesis.

The characterization of CH_4 and H_3^+ species, simultaneously observed with JIRAM, is finally important for better constraining the atmospheric models of Jupiter and understanding the planetary formation.

Acknowledgment. The JIRAM project is funded by the Italian Space Agency (ASI). In particular, this work has been developed under the agreement 2016-23-H.0

The original JIRAM data used for this work are available at the NASA Planetary Data System website

https://pds-atmospheres.nmsu.edu/data_and_services/atmospheres_data/JUNO/jiram.html.

The Maps in Figure 4, 5 and 6 were produced by using the commercial software ENVI (https://www.harrisgeospatial.com/Software-Technology).

The analysis has been done using homemade procedure based on IDL and Fortran languages.

Repository for the data products reported in this study is: https://doi.org/10.5281/zenodo.5658387

References

Acton, C. H. (1996). Ancillary data services of NASA's Navigation and Ancillary Information Facility. *Planetary. and Space Science*, 44(1), 65–70. https://doi.org/10.1016/0032-0633(95)00107-7

Adriani, A., Filacchione, G., Di Iorio, T., et al. (2017). JIRAM, the Jovian infrared Auroral mapper. *Space Science Reviews,* 213, 393. https://doi.org/10.1007/s11214-014-0094-y

Adriani, A., Mura, A., Moriconi, M.L., et al. (2017). Preliminary JIRAM results from Juno polar observations: 2. Analysis of the Jupiter southern H_3^+ emissions and comparison with the north aurora. *Geophysical Research Letters,* 44. https://doi.org/10.1002/2017GRL072905

Altieri, F., Dinelli, B.M., Migliorini, A., et al. (2016). Mapping of hydrocarbons and H_3^+ emissions at Jupiter's north pole using Galileo/NIMS data. *Geophysical Research Letters,* 43, 11558-11566. https://doi.org/10.1002/2016GL070787

Atreya, S. K. (1987). Atmospheres and ionospheres of the outer planets and their satellites. *Springer*, New York-Heidelberg, pp 47-48, 76-77 and 138-142.

646 Atreya, S. K., Wong, M.H., Owen, T.C., Mahaffy, P.R., Niemann, H.B., de Pater, I., et al. (1999). A
647 Comparison of the atmospheres of Jupiter and Saturn: Deep atmospheric composition, cloud structure, vertical
648 mixing, and origin. *Planteary. and Space Science*, 47, 1243–1262.

649

650 Ballester, G.E., Miller, S., Tennyson, J., Trafton, L.M., and Geballe, T.R. (1994). Latitudinal temperature
651 variations of Jovian H_3^+. *Icarus,* 107, 189-194.

652

653 Bolton, S.J., Levin, S., Janssen, M., Oyafuso, F.A., Zhang, Z., Li, C., et al. (2019). Initial results of
654 Juno's Microwave Imaging of Jupiter's atmosphere at multiple depths. P21G-3455, *AGU Fall meeting*, San
655 Francisco, 7-13 December 2019.

656

657 Bonfond, B., Gladstone, G.R., Grodent, D., Greathause, T.K., Versteeg, M.H., Hue, V., et al. (2017).
658 Morphology of the UV aurorae Jupiter during Juno's first perijove observations. *Geophysical Research*
659 *Letters.* https://doi.org/10.1002/2017GL073114

660

661

662 Bougher, S.W., Waite, J.H., Majeed, T., Gladstone, G.R. (2005). Jupiter Thermospheric General
663 Circulation Model (JTGCM): Global structure and dynamics driven by auroral and Joule heating. *Journal of*
664 *Geophysical Research: Planets,* 110, E04008.

665

666 Caldwell, J., Tokunags, A.T., Orton, G.S. (1983). Further observations of 8-μm polar brightenings of
667 Jupiter. *Icarus,* 53, 133-140.

668

669 Caldwell, J., Halthore, R., Orton, G., Berstralh, J. (1988). Infrared polar brightenings on Jupiter VI.
670 Spatial properties of methane emission. *Icarus,* 74, 331-339.

671

672 Carlotti, M., (1988). Global-fit approach to the analysis of limb-scanning atmospheric measurements.
673 *Applied Optics,* 27, 3250-3254.

674

675 Clarke, J.T., Ajello, J., Ballester, G., et al. (2002). Ultraviolet emissions from the magnetic footprints of
676 Io, Ganymede, and Europa on Jupiter. *Nature*, 415, 997-1000.

677

678 Connerney, J.E.P., Waite, J.H. (1984). Images of excited H_3^+ at the foot of Io flux tube in Jupiter's
679 atmosphere. *Science*, 262, 2471-2483.

680

681 Connerney, J.E.P., Baron, R., Satoh, T., Owen, T. (1993). Images of excited H_3^+ at the foot of the Io flux
682 tube in Jupiter's atmosphere. *Science,* 262, 1035-1038.

683

684 Cosentino, R.G., Morales-Juberias, R., Greathouse, T., Orton, G., Johnson, P., Fletcher, L.N., Simon, A.
685 (2017). New observations and modeling of Jupiter's quasi-quadrennial oscillation, *Journal of Geophysical*
686 *Research*, 122, 2719-2744. https://doi.org/10.1002/2017JE005342

687

688 Dinelli, B.M., Fabiano, F., Adriani, A., et al. (2017). Preliminary JIRAM results from Juno polar
689 observations: 1. Methodology and analysis applied to the Jovian northern polar region, *Geophysical Research*
690 *Letters,* 44. https://doi.org/10.1002/2017GRL072929

691

692 Dinelli, B.M., Adriani, A., Mura, A., Altieri, F., Migliorini, A., Moriconi, M.L. (2019). JUNO/JIRAM's
693 view of Jupiter's H_3^+ emissions. *Philosophical Transaction of the Royal Society A*.

694

695 Drossart, P., Maillard, J.-P., Cladwell, S.J., et al. (1989). Detection of the H_3^+ on Jupiter. *Nature,* 340,
696 539-541. https://doi.org/10.1038/340539a0

697

Drossart, P., Bezard, B., Atreya, S., et al. (1993). Thermal profiles in the auroral regions of Jupiter. *Journal of Geophysical Research,* 98, 18803-18812. https://doi.org/10.1029/93JE01801

Gérard, J.-C., Mura, A., Bonfond, B., Gladstone, G.R., Adriani, A., et al. (2018). Concurrent ultraviolet and infrared observations of the north Jovian aurora during Juno's first perijove. *Icarus,* 312, 145-156.

Giles, R.S., Fletcher, L.N., Irwin, P.G.J., et al. (2016). Detection of H_3^+ auroral emission in the Jupiter's 5-micron window. *Astronomy &. Astrophysics,* 589, A67, https://doi.org/10.1051/0004-6361/201628170.

Gordon, I.E., Rothman, L.S., Hill, C., et al. (2017). The HITRAN2016 Molecular Spectroscopic Database. *Journal of Quantitative Spectroscopy & Radiative Transfer*, 203, 3-69.

Grodent, D., Waite, Jr. J.H., Gérard, J.C. (2001). A self-consistent model of the Jovian auroral thermal structure. *Journal of Geophysical Research,* 106, 12, 933-12, 952. https://doi.org/10.1029/2000JA900129

Hunten, D.M., Dessler, A. J. (1977). Soft electrons as a possible heat source for Jupiter's thermosphere. *Planeary. and Space Science,* 25, 817-821.

Kim, S.J., Caldwell, J., Rivolo, A.R., Wagener, R., Orton, G.S. (1985). Infrared polar brightening on Jupiter III. Spectrometry from the Voyager 1 IRIS experiment. *Icarus,* 64, 233-248. https://doi.org/10.1016/0019-1035(85)90088-0

Kim, S.J., Drossart, P., Caldwell, J., et al. (1991). Images of aurorae on Jupiter from H_3^+ emission at 4 μm. *Nature,* 353, 536-539. https://doi.org/10.1038/353536a0

Kim, S.J., Geballe, T.R., Seo, H.J., Jim, J.H. (2009). Jupiter's hydrocarbon polar brightening: Discovery of 3-micron line emission from south polar CH_4, C_2H_2 and C_2H_6. *Icarus,* 202, 354-357. https://doi.org/10.1016/j.icarus.2009.03.020

Kim, S.J., Sim, C.K., Sohn, M.R., Moses, J.I. (2014). CH_4 mixing ratios at microbar pressure levels of Jupiter a constrained by 3-micron ISO data. *Icarus,* 237, 42-51. https://doi.org/10.1016/j.icarus.2014.04.023

Kim, S.J., Sim, C.K., Ho, J., et al. (2015). Hot CH_4 in the polar regions of Jupiter, *Icarus* 257, 217-220. https://doi.org/10.1016/j.icarus.2015.05.008

Koskinen, T.T., Aylaward, A.D., Miller, S. (2007). A stability limit for the atmospheres of giant extrasolar planets. *Nature*, 412, 891.

Lam, H.A., Achilleos, N., Miller, S., et al. (1997). A baseline spectroscopic study of the infrared auroras of Jupiter. *Icarus* 127, 379-393.

Li, C., Ingersoll, A., Janssen, M., et al. (2017). The distribution of ammonia on Jupiter from a preliminary inversion of Juno microwave radiometer data. *Geophysical Research Letters,* 44, 5317-5325. https://doi.org/10.1002/2017GL073159

Li, C., Ingersoll, A., Bolton, S., Levin, S., Janssen, M., Atreya, S., et al. (2020). The Water Abundance in Jupiter's Equatorial Zone. *Nature Astronomy* 2020. https://doi.org/10.1038/s41550-020-1009-3

Lindsay, C.M. and McCall, B.J. (2001). Comprehensive evaluation and compilation of H_3^+ spectroscopy. *J. Mol. Spectrosc.*, 60-83. https://doi.org/10.1006/jmsp.2001.8444

Lystrup, M.B., et al. (2008). First vertical ion density profile in Jupiter's auroral atmosphere: direct observations using the Keck II telescope. *Astrophysical Journal,* 677, 790-797. https://doi.org/10.1086/529509

Marten, A., De Bergh, C., Owen, T., Gautier, D., Maillard, J.-P., Drossart, P., et al. (1994). Four-micron high-resolution spectra of Jupiter in the North Equatorial Belt: H_3^+ emissions and the $^{12}C/^{13}C$ ratio. *Planeary. and Space Science*, 42, 391-399.

Miller, S., Achilleos, N., Ballester, G., et al. (1997). Mid-to-low latitude H_3^+ emission from Jupiter. *Icarus,* 130, 57-65.

Miller, S., Tennyson, J., Geballe, T.R., Stallard, T.S. (2020). Thirty years of H_3^+ astronomy, *Reviews of Modern Phys*ics, 92. https://doi.org/10.1103/RevModPhys.92.035003

Migliorini, A., Dinelli, B.M., Moriconi, M.L., et al. (2019). H_3^+ characteristics in the Jupiter atmosphere as observed at limb with Juno/JIRAM. *Icarus,* 329, 132-139. https://doi.org/10.1016/j.icarus.2019.04.003

Moore, L., Melin, H., O'Donoghue, J., Stallard, T., Moses, J., Galand, M., Miller, S., Schmidt, C. (2019). Modelling H_3^+ in planetary atmospheres: effects of vertical gradients on observed quantities. *Philosophical Transaction of the Royal Society A*, arXiv:1904.04284v2.

Moriconi, M.L., Adriani, A., Dinelli, B.M., et al. (2017). Preliminary JIRAM results from Juno polar observations: 3. Evidence of diffuse methane presence in the Jupiter auroral regions. *Geophysical Research Letters,* 44, 4641-4648. https://doi.org/10.1002/2017GL073592

Moses, J.I., Fouchet, T., Bézard, B., Gladstone, G.R., Lellouch, E., Feuchtgruber, H. (2005). Photochemistry and diffusion in Jupiter's stratosphere: Constraints from ISO observations and comparisons

776 with other giant planets. *Journal of Geophysical Research,* 110, E08001.
777 https://doi.org/10.1029/2005JE002411

778

779 Mura, A., Adriani, A., Altieri, F., et al. (2017). Infrared observations of Jovian aurora from Juno's first
780 orbit: main oval and satellite footprints. *Geophysical Research Letters,* 44.
781 https://doi.org/10.1022/2017GRL072954

782

783 Mura, A., Adriani, A., Altieri, F., et al. (2018). Juno observations of spot structures and a split tail in Io-
784 induced aurorae on Jupiter. *Science*, 361, 774-777. https://doi.org/10.1126/science.aat1450

785

786 O'Donoghue, J., Moore, L., Stallard, T.S., Melin, H. (2016). Heating of Jupiter's upper atmosphere
787 above the Great Red Spot. *Nature*, 536, 190-192. http://dx.doi.org/10.1038/nature18940

788

789 Ray, L.C., Lorch, C.T.S., O'Donoghue, J., Yates, J.N., Badman, S.V., Smith, C.G.A., Stallard, T.S. (2019).
790 Why is the H3+ hot spot above Jupiter's Great Red Spot so hot? *Philosophical Transaction of the Royal Society*
791 *A,* 377. http://dx.doi.org/10.1098/rsta.2018.0407

792

793 Rodgers, C.D. (2000). Inverse method for atmospheric sounding: Theory and practice. *In: World*
794 *Scientific*, (Singapore).

795

796 Sada, P.V., et al. (2003). Transient IR phenomena observed by Cassini/CIRS in Jupiter's auroral regions.
797 *Bulletin of the American Astronomical Society,* 35, 402.

798

799 Seiff, A. (1998). Thermal structure of Jupiter's atmosphere near the edge of a 5-μm hot spot in the north
800 equatorial belt. *Journal of Geophysical Research,* 103, 22857-22889.

801

802 Stallard, T.S., Melin, H., Miller, S., et al. (2015). Cassini VIMS observations of H_3^+ emission on the
803 nightside of Jupiter. *Journal of Geophysical Research: Space Physics,* 120, 6948-6973.
804 https://doi.org/10.1002/2015JA021097

805

806 Stallard, T.S., Melin, H., Miller, S., Moore, L., O'Donoghue J., Connerney, J.E.P., et al. (2017). The
807 great cold spot in Jupiter's upper atmosphere. *Geophysical Research Letters,* 44, 3000.

808

809 Stallard, T.S., Burrell, A., Melin, H., et al. (2018). Identification of Jupiter's magnetic equator within H_3^+
810 ionospheric emission. *Nature Astron.* 2, 773-777. https://doi.org/10.1038/s41550-018-0523-z

811

812 Uno, T., Yasaba, Y., Tao, C., et al. (2014). Vertical emissivity profiles of Jupiter's northern H_3^+ and H_2
813 infrared auroras observed by Subaru/IRCS. *Journal of Geophysical Research: Space Physics,* 119, 10219-
814 10241. https://doi.org/10.1002/2014JA020454